A multiscale approach to ion diffusion in clays: Building a two-state diffusion–reaction scheme from microscopic dynamics

Benjamin Rotenberg, Virginie Marry, Jean-François Dufrêche, Eric Giffaut, Pierre Turq

▶ **To cite this version:**

Benjamin Rotenberg, Virginie Marry, Jean-François Dufrêche, Eric Giffaut, Pierre Turq. A multiscale approach to ion diffusion in clays: Building a two-state diffusion–reaction scheme from microscopic dynamics. Journal of Colloid and Interface Science, 2007, Elkin 06, International Electrokinetics Conference, June 25-29, Nancy, France, 309 (2), pp.289 - 295. 10.1016/j.jcis.2007.01.090 . hal-01917520

HAL Id: hal-01917520

https://hal.sorbonne-universite.fr/hal-01917520

Submitted on 9 Nov 2018

HAL is a multi-disciplinary open access archive for the deposit and dissemination of scientific research documents, whether they are published or not. The documents may come from teaching and research institutions in France or abroad, or from public or private research centers.

L'archive ouverte pluridisciplinaire **HAL**, est destinée au dépôt et à la diffusion de documents scientifiques de niveau recherche, publiés ou non, émanant des établissements d'enseignement et de recherche français ou étrangers, des laboratoires publics ou privés.

Manuscript for ELKIN06 - JCIS special issue

A multiscale approach to ion diffusion in clays : Building a two-state diffusion-reaction scheme from microscopic dynamics

Benjamin Rotenberg[1,2,*], Virginie Marry[1],
Jean-François Dufrêche[1], Eric Giffaut[2] and Pierre Turq[1]

rotenber@ccr.jussieu.fr
+33 (0)144273118 (fax: 3228)

[1] *Université Pierre et Marie Curie-Paris6,*
Laboratoire Liquides Ioniques et Interfaces Chargées,
UMR CNRS 7612, 4 pl. Jussieu, Paris F-75005 and

[2] *ANDRA, Parc de la Croix Blanche, 1/7 rue Jean Monnet,*
92298 Châtenay Malabry cedex, F-75005 France

Abstract

The mobility of particles is generally lowered by the presence of a confining medium, both because of geometrical effects, and of the interactions with the confining surfaces, especially when the latter are charged. The water/mineral interface plays a central role in the dynamics of ions: The ionic mobility in clays is often understood as an interplay between the diffusion of mobile ions and their possible trapping at the mineral surfaces.

We describe how to build a two-state diffusion-reaction scheme from the microscopic dynamics of ions, controlled by their interaction with a mineral surfaces. The starting point is an atomic description of the clay interlayer using molecular simulations. These provide a complete description of the ionic dynamics on short time- and lengthscales. Using the results of these simulations, we then build a robust mesoscopic (Fokker-Planck) description. In turn, this mesoscopic description is used to determine the mobility of the ions in the interlayer. These results can then be cast into a diffusion-reaction scheme, introducing in particular the fraction of mobile ions, or equivalently the distribution coefficient K_d. This coefficient is of great importance in characterizing electrokinetic phenomena in porous materials.

PACS numbers:

Keywords: clay, ion transport, diffusion, two-state, multiscale, coarse-graining

1. INTRODUCTION

Electrokinetic phenomena are related to the transport properties of mobile charged species (ions) near charged surfaces (e.g. colloids or macroscopic mineral surfaces). The presence of solid surfaces influences dramatically the ionic mobility, especially in porous media such as compacted clays, where geometrical confinement is reinforced by the interactions between the ionic species and the charged surfaces. This retention property has made clayey materials good candidates for the long term storage of chemical and nuclear waste, which often contain charged species.

The water/mineral interface plays a central role in the overall dynamics of ions, which is usually described using the sorption concept: An ion can be trapped temporarily, immobilized for some time, thereby reducing its mobility. The extensive literature on the related sorption data (empirical partitioning coefficients K_d) obtained by geologists and engineers provide a convenient tool for the modeling and prediction of ion mobility in these materials [1–4]. On the microscopic scale however, there is no clear-cut distinction between trapped and mobile ions. In compacted clays, the water content is very low, and there has been some evidence that the usual macroscopic equations (e.g. Navier-Stokes for solvent flow, Poisson-Boltzmann for ionic distributions) are at the limit of their validity [5]. A detailed description of ionic mobility is still at hand, however, using Molecular Dynamics (MD) simulations [6–10]. They provide an atomically resolved description of ion (and water) motion near the mineral surfaces, and allow for the computation of the short-time diffusion coefficient of ions.

The purpose of the present paper is to provide a link between the molecular simulations and the simplified diffusion-reaction picture, by an appropriate coarse-graining strategy. In section 2, we highlight some MD results on ionic diffusion in clay interlayers. These results are then used in section 4 to build a robust mesoscopic (Fokker-Planck) description, in which the interactions of the ions with the surfaces are introduced as an effective external potential, and the interactions of the ions with the solvent are described by a unique friction parameter. In turn, the mesoscopic model is used in section 5 to build a diffusion-reaction scheme, by first determining the mobility of the ions in the interlayer as a function of the strength of their interaction with the surface. These results are eventually cast into a diffusion-reaction scheme, introducing in particular the fraction of mobile ions, or equivalently the distribution

coefficient K_d.

2. MOLECULAR MODELING OF COMPACTED CLAYS

The most detailed information on water and ion dynamics in clay interlayers can be obtained by molecular modeling, which provides an atomically resolved description of the system. Molecular simulations are done for a montmorillonite clay model whose unit cell formula is $M_{0.75}$ Si_8 $(Al_{3.25}$ $Mg_{0.75})$ O_{20} $(OH)_4$, where M is the counterion. Clay particles are formed by stacks of aluminosilicate layers. Each layer of montmorillonite consists of three sheets : An octahedral sheet of Al oxide between two tetrahedral sheets of Si oxide (see figure 1). Substitutions of Al^{III} by Mg^{II} give rise to a negative charge on the mineral compensated by cations (M). The above clay is an idealized montmorillonite which is close to the natural clay MX80 studied for its potential applications for the geological storage of nuclear waste [11, 12]. The simulations are done with Li^+, Na^+, K^+ and Cs^+ counterions. Na^+ is one of the major natural cations in MX80 (with Ca^{2+}) and Cs^+ is a potential radionuclide. Li^+ and K^+ are also studied to complete the comparison of diffusion properties of the alkali cations.

The parameters used in the interaction potentials are taken from literature and detailed in previous articles [8, 9]. For the counterions, we use the Lennard-Jones parameters of Koneshan [13]. The simulation box contains two clay layers of eight unit cells each. The positions of the clay atoms are taken from X-ray data [14]. The lateral dimensions of the layer are then 20.72×17.94 Å^2, its thickness 6.54 Å. At low relative humidities, water can enter in the interlayer in order to solvate the counterions and form one, two or three layers of water in the interlayers, depending on the compaction, humidity and the type of counterion. Only the monohydrated state is simulated, here with $N = 36$ water molecules in each interlayer space, *i.e.* 6 water molecules per counterion. In this case, the space is too constrained for the cation to be fully hydrated by water. Hence cations are always in direct contact with the surface clay atoms. A snapshot of the simulation box is given in figure 1.

Prior to dynamic studies, the average interlayer spacings for each type of cation is evaluated by Monte Carlo simulations in the (N, σ_{zz}=1 bar, T=298 K) ensemble. We found 12.25 Å, 12.3 Å, 12.4 Å and 12.7 Å for Li^+, Na^+, K^+ and Cs^+ respectively. These results agree with RX diffraction experiments [15–18] and other simulations on montmorillonites

[19–22]. After equilibration, the interlayer structural properties are calculated by fixing interlayer spacings at their average value. Moreover, the hexagonal cavities formed by silicon and oxygen atoms of opposite surfaces are maintained face to face during the simulations. This allows an easier interpretation of the preferential paths of the cations along the surface of the clay layer. All MD simulations were performed using the DLPOLY software. A timestep of 1 fs was used, and a set of 720 ps simulations was carried out for each cation (2 to 4 runs per cation). Simulations were done in the NVT ensemble, with T=298 K, using a Nosé-Hoover thermostat.

Water and cation distributions in the direction perpendicular to the clay surface are shown on figure 2 for one interlayer space. The peak of water oxygen atoms widens with increasing size of the cation and even starts to split in the case of K^+ and Cs^+. The opposite is observed for the cation distributions. An obvious explanation is that the distance between surfaces is controled by the size of the largest species. In the case of small cations, the size of the water molecule is determining and the interlayer spacings remain around 12.3 Å : The cations are free to go from one surface to another according to their interactions with the surface atoms and their hydration state. In the case of large cations, the size of the cation becomes more important and the water moves perpendicular to the clay surface more easily.

It is already known that alkali cations have different behaviours towards water and clay surfaces. Experimentally, Na- and Li-montmorillonites can swell until the tri-hydrated state (three water layers in the interlayer space) under increasing humidity, although Cs- and K-montmorillonites can only reach the monohydrated state [15]. Simulations show that in the bihydrated case, Na^+ remains in the middle of the interlayer space, surrounded by six water molecules, like in its first hydration shell in bulk water [9]. On the contrary, Cs^+ remains close to the clay surface, even in a fictitious bihydrated state. The maps of their preferential positions along the clay surface in the monohydrated state are given on figure 3 with those of Li^+ and K^+. They illustrate the different behaviour of the alkali cations. Large cations (Cs^+ and K^+) exhibit a site-to-site diffusion above surface silicon atoms. They complete their solvation shell with the three oxygen atoms linked to the silicon. Small cations (Na^+ and Li^+) prefer oxygen surface atoms to silicon and hexagonal cavity centers. A previous study showed that when the clay layers are allowed to move horizontally (in the two directions parallel to the surfaces) the hexagonal cavities silicon atoms are preferentially facing each other in the case of Cs-montmorillonite. It is not the

case with Na-montmorillonite. However, even with another relative shift of the hexagonal cavities, a preference of Na^+ for surface oxygen atoms was already observed [8].

3. COARSE-GRAINING STRATEGY

Molecular simulations provide a picture of water and ion dynamics in clays on short timescales (ns) and small lengthscales (nm). On the macroscopic scale of observation, and for engineering purposes, these molecular details are not necessary, and a coarser representation at the macroscopic scale (>mm) is generally adopted. In order to link this microscopic information to macroscopic observables, and especially to the apparent diffusion coefficient of each species, one usually separates the geometrical confinement effect from the physical interactions with the mineral surfaces. For the geometrical part, a set of empirical parameters is introduced : Porosity ϵ, constrictivity δ and tortuosity τ. Porosity is the fraction of the volume accessible to the diffusive species. Constrictivity is a geometrical factor accounting for the closing/opening of diffusion pathways: $\delta > 1$ if the pore width increases along the diffusion path, $\delta < 1$ in the opposite case [23–25]. Tortuosity quantifies the length of the diffusion pathways in the medium with respect to a straight trajectory. Only ϵ and the ratio δ/τ^2 are available experimentally. In addition to geometrical effects, the interactions of the diffusing particles with the mineral surfaces are accounted for in the framework of a diffusion-reaction scheme. An ion can remain temporarily trapped at the mineral surface, thereby reducing its apparent diffusion coefficient, according to the "chemical" reaction :

$$\text{mobile} \rightleftharpoons \text{adsorbed} \tag{1}$$

This mechanism is quantified by a partitioning coefficient K_d, which is the ratio between the concentrations of bound and mobile forms of each chemical species. At the macroscopic scale, the apparent diffusion coefficient is deduced from the "free" diffusion coefficient D_0 using :

$$D_a = D_0 \times \frac{\delta}{\tau^2} \times \frac{\epsilon}{(\epsilon + \rho K_d)} \tag{2}$$

with ρ the dry density of the medium.

As mentioned earlier, there is no clear-cut distinction on the molecular scale between mobile and bound ions. Therefore, the definition of a diffusion-reaction model from the microscopic dynamics (as obtained by MD simulations) is not without its ambiguities. We now

suggest a tentative method to connect the atomic level of modeling developed in section 2 to the more approximate one just described. The general coarse-graining strategy involves two steps. The first one defines a mesoscopic description, calibrated on the molecular dynamics results, *i.e.* taking advantage of the microscopic insights gained from molecular modeling. The solvent is described as a continuum, and the ion/surface interaction is included as an effective potential. The second step derives, from the mesoscopic model, the parameters defining the diffusion-reaction scheme, namely a dimensionless analogue of K_d, and the kinetic rates of exchange. Section 4 describes the first step, while the second is postponed to section 5.

4. MESOSCOPIC DESCRIPTION

This section describes how to calibrate the continuous solvent description of the interlayer on MD simulations. Such an approach uses the actual results on the complex system (described in section 2) instead of an infinite dilution reference.

When the solute (ion) moves slower than the solvent (water) one can average over the solvent degrees of freedom [26], and describe the solute/solvent interaction by a single friction parameter γ (in s^{-1}) : The friction force on an ion is proportional to its velocity ($\mathbf{F}_{solv} = -m\gamma\mathbf{v}$), and the resulting diffusion coefficient is given by Einstein's relation $D_0 = v_T^2/\gamma$, with $v_T = \sqrt{k_B T/m}$ the thermal velocity of the ion. The value of the friction can be extracted from MD simulations using a fit of the velocity auto-correlation function (VACF) [27]:

$$Z(t) = \frac{1}{3}\langle \mathbf{v}(t) \cdot \mathbf{v}(0) \rangle = \frac{k_B T}{m} \exp(-\gamma t) \tag{3}$$

The right-hand side is the analytical form for Brownian motion, and the VACF is obtained by analysis of the MD trajectories. A typical value for Cs^+ is $\gamma \sim 5$ ps^{-1}. However, the final results of our approach on the definition of K_d, do not depend on the precise value of γ. This point will be discussed in section 5.

The interaction of the ion with the mineral surface is introduced as an external (free energy) potential V, which can be computed by an inversion procedure from the ionic density profiles obtained by molecular dynamics simulations. The solute dynamics is then characterized by the time evolution of the probability density function $f(\mathbf{x}, \mathbf{v}, t)$ of finding an ion at a given position with a given velocity. The moments of f in velocity space are the

ionic density and flux :

$$\rho(\mathbf{x},t) \;=\; \int f(\mathbf{x},\mathbf{v},t)\;\mathrm{d}\mathbf{v} \tag{4}$$

$$\mathbf{j}(\mathbf{x},t) \;=\; \int f(\mathbf{x},\mathbf{v},t)\mathbf{v}\;\mathrm{d}\mathbf{v} \tag{5}$$

This probability density evolves, within this simplified mesoscopic description, according to the Fokker-Planck (FP) equation [28] :

$$\partial_t f + \mathbf{v}\cdot\nabla f = \nabla_{\mathbf{v}}\cdot\left(\gamma\mathbf{v} + \frac{\nabla V}{m} + \frac{\gamma k_B T}{m}\nabla_{\mathbf{v}}\right) f \tag{6}$$

The potential V encompasses all interactions involving the ion (except from the ion/water interaction, which is the friction): In addition to the ion/surface interaction, it can also include an external field (*e.g.* an electrical field), which is necessary to determine the mobility of the ions. To solve the FP equation numerically, we used a lattice method inspired by the Lattice-Boltzmann methodology: The lattice Fokker-Planck method [29–32].

In order to investigate efficiently the effect of surface-ion interactions on ionic mobility (and later on the parameters of the two-state model), we did not use a potential directly derived from MD simulations, and used instead an analytical ansatz, which respects the characteristic features of the true potential (topology, barrier height, ...). The magnitude of the ion/surface interactions is quantified by the ratio $V_s/k_BT = \beta V_s$, where V_s is the barrier connecting two adjacent free energy minima. The precise form of the potential is given by:

$$V(x,y) = V_s \times \left[3 + 2\cos\frac{2\pi}{a}\left(x + \frac{y}{\sqrt{3}}\right) + 2\cos\frac{2\pi}{a}\left(x - \frac{y}{\sqrt{3}}\right) + 2\cos\frac{2\pi}{a}\left(\frac{2y}{\sqrt{3}}\right)\right] \tag{7}$$

with a the distance between two maxima ($a \sim 5.2$ Å for montmorillonite).

The density profiles corresponding to this model potential are the steady state solutions of equation 6 with V given by equation 7. The solution statisfies the Boltzmann law: $\rho(x,y) \propto \exp(-\beta V(x,y))$. Results are shown in figure 4. These profiles are to be compared to those obtained with the fully atomic description of figure 3: The K^+ and Cs^+ behaviours are relatively well reproduced for the intermediate (b) and high (c) values of βV_s. There is clearly room for improvement in the Na^+ case (a), although it already reflects its more diffuse behaviour. One should keep in mind that in the Li^+ and Na^+ cases the hydration tendency is rather different from the K^+ and Cs^+ cases, and that the results of section 2 were obtained for the monohydrated state only, with the constraint of face-to-face clay layers. In

this situation, Li^+ (and to a smaller extent Na^+) tend to avoid the center of the interlayer (see the two peaks on figure 2), so that a strictly two dimensional modeling as the one undertaken here is not fully appropriate. The study of the bihydrated state, in which Li^+ and Na^+ are clearly located in the midplane of the interlayer [20, 33] is under progress. This will open the way to the study of more hydrated states.

5. IONIC MOBILITY AND THE DIFFUSION-REACTION SCHEME

The second coarse-graining step consists in the definition of the two-state model from the mesoscopic (FP) description. The underlying idea is that in such a model, the reduction in mobility is traced back to the fixation of some ions on a surface: only a fraction f_m is considered as mobile. The link between microscopic mobility and two-state model is thus provided by the equality $f_m = \mu_{app}/\mu_0$, where $\mu_0 = 1/\gamma$ is the "free" mobility of the ions, that is when no interactions with the surfaces are present.

Thus we first need to determine the mobility of the ions interacting with the mineral surfaces. This is achieved by applying an external force $\mathbf{F}_{ext}$ on the ions, in addition to the one arising from the clay layer itself. In practice, equation 6 is now solved with $(\nabla V - \mathbf{F}_{ext})/m$ on the right-hand side. At steady-state, the average velocity is proportional to the applied field, the proportionality coefficient being related to the apparent mobility : $\mathbf{v_{st}} = \mu_{app}/m \times \mathbf{F}_{ext}$. The latter is of course lower than the "free" mobility μ_0. The mobility μ_{app} is reported as a function of βV_s in figure 5. The value is rescaled by μ_0. The two components of the mobility tensor, obtained by applying the force along each direction, are equal. Isotropy of the mobility is a known consequence of the symmetry of the honeycomb lattice [34, 35]. As expected, the mobility decreases with increasing affinity for the surface (increasing βV_s). Two regimes are observed, with a crossover at approximately $\beta V_s \sim 1$. Their significance will be discussed below, when interpreted in terms of K_d.

Within the two-state diffusion-reaction scheme, the ratio μ_{app}/μ_0 is precisely the fraction of mobile ions f_m, that is the ions that are not bound to the surfaces. Translating this fraction of mobile ions in terms of the partioning coefficient K_d, one obtains :

$$K_d = \frac{1 - f_m}{f_m} = \frac{\mu_0 - \mu_{app}}{\mu_{app}} \tag{8}$$

Note that the definition of K_d is slightly different from the one given above, because no

geometrical effects are included in the present description. In particular, this definition makes K_d dimensionless. Our purpose is to give a microscopic basis to a simple two-state model, which is generally the starting point of even coarser models, such as the one presented in section 3. The simplicity of the latter allows to include other features of the real material (distribution of porosity sizes, presence of minerals other than clay, ...) which are out of the scope of the present study. Equation 8 clearly shows that K_d only depends on the ratio μ_{app}/μ_0. In our simple model, which neglects ionic correlations, and in the high friction limit (the one relevant here), this ratio is in fact independent of the value of the friction γ, as was mentioned earlier.

Results for K_d as a function of the interaction parameter βV_s are represented on a logarithmic scale in figure 6. The two regimes appear now more obviously : For strong interactions with the walls or at low temperature, the diffusion follows an Arrhenius law, with an activation energy of V_s, the barrier that an ion needs to overcome to move from one energy minimum to the next; for weak interactions or at high temperature, no such activated diffusion is seen. These results are consistent with the trajectories observed in MD simulations for sodium (weak interaction case) and cesium (strong interaction case).

From the knowledge of the amount of bound ions, it is also possible to determine: (a) the localization of the bound and mobile states, and (b) the adsorption/desorption rates, thereby completely specifying the diffusion-reaction model [35]. The results, not shown, indicate that the border between fixed and mobile ions is independent of the precise value of βV_s, provided that the latter is large enough (that is, for strong affinity for the surface). This justifies the notion of trapping site, because it makes reference to the mineral surface only, and not to the ions moving in its vicinity. We refer the interested reader to a previous publication [35].

6. CONCLUSION

We have demonstrated how a two-state diffusion-reaction model can be developed from the microscopic dynamics of ions in compacted clays, following a two step coarse-graining strategy. Molecular dynamics simulations first provide the information which is necessary to calibrate a mesoscopic description of the clay/ion/water system. The latter allows for a determination of ionic mobility near the clay surface, which in turn can be translated in

terms of the diffusion-reaction scheme *via* the fraction of mobile ions f_m, or equivalently the distribution coefficient K_d.

This coarse-graining strategy extends the continuous solvent description used in the theory of bulk electrolyte solution since Debye, Hückel and Onsager [36] to non infinitely diluted reference states. It is of course not restricted to clays, and applies to any charged surfaces. A generalization of the method is needed if one wants to consider semi-infinite systems (that is a surface facing a bulk fluid), as opposed to the confined, quasi two-dimensional system of a clay interlayer. However we expect no particular difficulty, except for the computational cost of solving the FP equation in three dimesions. The method used in this paper, lattice Fokker-Planck, is a method of choice to overcome this technical difficulty.

Acknowledgments

BR acknowlegdes financial support from ANDRA (Agence Nationale pour la Gestion des Déchets Radioactifs). Financial support of GdR PARIS (Physico-chimie des Actinides et autres Radioéléments aux Interfaces et en Solution) is gratefully acknowledged. LI2C is part of the SFR Sciences Chimiques pour l'Analyse et la Mesure de Paris-Centre.

[1] ANDRA, *Référentiel Matériaux*, vol. 1 : Matériaux à base d'argiles gonflantes (2005).

[2] C. Daqing, T. Eriksen, Radio. Acta **82**, 287 (1998).

[3] T. Eriksen, M. Jansson, M. Molera, Eng. Geol. **54**, 231 (1999).

[4] M. Molera, T. Eriksen, Radio. Acta **90**, 753 (2004).

[5] J.-F. Dufrêche, V. Marry, O. Bernard, and P. Turq, Coll. Surf. A **195**, 171 (2001).

[6] N. T. Skipper, G. Sposito, F.-R. C. Chang, Clays Clay Miner. **43**, 294 (1995).

[7] F.-R. C. Chang, N.T. Skipper, G. Sposito, Langmuir **11**, 2734 (1995).

[8] V. Marry, P. Turq, T. Cartailler, and D. Levesque, J. Chem. Phys **117**, 3454 (2002).

[9] V. Marry, F. Grün, C. Simon, M. Jardat, P. Turq, and C. Amatore, J. Phys. : Condens. Matter **14**, 9207 (2002).

[10] R. Sutton and G. Sposito, J. Colloid Interface Sci. **237**, 174 (2001).

[11] ANDRA, *Évaluation de la faisabilité du stockage géologique en formation argileuse*, vol. Dossier 2005 Argile : Synthèse (ANDRA, Châtenay-Malabry, France, 2005).

[12] M. Bradbury, B. Baeyens, *Near Field Sorption Data Bases for Compacted MX-80 Bentonite for Performance Assesment of a High-Level Radioactive Waste Repository in Opalinus Clay Host Rock* (2003).

[13] S. Koneshan, C. Rasaiah, R. Lynden-Bell, and S. Lee, J. Phys. Chem. B **102**, 4193 (1998).

[14] G. W. Brindley and G. Brown, *Crystal Structures of Clay Minerals and their X-ray Identification* (Mineralogical Society, London, 1980).

[15] I. Bérend, J.M. Cases, M. Francois, J.P. Uriot, L.J. Michot, A. Masion, F. Thomas, Clays and Clay Minerals **43**, 324 (1995).

[16] R. Mooney, A. Keenan, and L. Wood, J. Am. Chem. Soc. **74**, 1371 (1952).

[17] R. Calvet, Ann. agron. **24**, 77 (1973).

[18] M. Fu, Z. Zhang, and P. Low, Clays Clay Miner. **38**, 485 (1990).

[19] F.-R. C. Chang, N. T. Skipper, G. Sposito, Langmuir **14**, 1201 (1998).

[20] F.-R. C. Chang, N. T. Skipper, G. Sposito, Langmuir **13**, 2074 (1997).

[21] F.-R. Chang, N. Skipper, and G. Sposito, Langmuir **11**, 2734 (1995).

[22] D. E. Smith, Langmuir **14**, 5959 (1998).

[23] H. Kato, M. Muroi, N. Yamada, H. Ishida, H. Sato, *Scientific basis for nuclear waste man-*

agement, vol. 18 (Materials Research Society, Pennsylvania, 1995).

[24] M. Ochs, M. Boonekamp, H. Wanner, H. Sato, M. Yui, Radiochimica Acta **82**, 437 (1998).

[25] M. Ochs, B. Lothenbach, H. Wanner, H. Sato, M. Yui, J. Contam. Hydrol. **47**, 283 (2001).

[26] P. M. V. Résibois, *Electrolyte Theory* (Harper & Row, 1968).

[27] J.-P. Hansen I. R. McDonald, *Theory of Simple Liquids, 3rd Edition* (Academic Press, 2006).

[28] H. Risken, *The Fokker-Planck Equation* (Springer-Verlag, Berlin, 1989).

[29] S. Melchionna, S. Succi, and J.-P. Hansen, Int. J. Mod. Phys. C **17**, 459 (2006).

[30] S. Melchionna, S. Succi, and J.-P. Hansen, Phys. Rev. E **73**, 017701 (2006).

[31] D. Moroni, B. Rotenberg, J.-P. Hansen, S. Succi, and S. Melchionna, Phys. Rev. E **73**, 066707 (2006).

[32] B. Rotenberg and D. Moroni, Phys. Rev. E **74**, 037701 (2006).

[33] E.J.M. Hensen, T. Tambach, A. Bliek, B. Smit, J. Chem. Phys. **115**, 3322 (2001).

[34] B. Bagchi, R. Zwanzig, M. C. Marchetti, Phys. Rev. A **31**, 892 (1985).

[35] B. Rotenberg, J.-F. Dufrêche, B. Bagchi, E. Giffaut, J.-P. Hansen, and P. Turq, J. Chem. Phys. **124**, 154701 (2006).

[36] J. M. G. Barthel H. Krienke W. Kunz, *Physical Chemistry of Electrolyte Solutions* (Springer, 1998).

FIG. 1: Snapshot of the simulation box for Cs-montmorillonite for the case of a water monolayer. Oxygen atoms are in red, H in white, Si in yellow, Al in green and Cs in blue. The interlayer distance corresponds to a water content of 6 water molecules per cation, a temperature of 298 K and a pressure of 1 bar (normal to clay layers).

FIG. 2: Top : Distributions of water oxygen atoms along the direction perpendicular to the clay surfaces. Bottom : Distributions of cations along the direction perpendicular to the clay surfaces for Li- (solid line), Na- (dashed), K- (dotted-dashed) and Cs-montmorillonite (dotted). The distance is given relative to the central layer midplane, and the distributions are in arbitrary units.

FIG. 3: Maps of cation distributions parallel to the clay surface for monohydrated Li-, Na-, K- and Cs-montmorillonites. The distributions are given for the elementary cell (containing one hexagonal cavity). Density increases with brightness. Dark and bright circles represent surface oxygen and silicon atoms respectively.

FIG. 4: Equilbrium ionic density $\rho(x, y) = \exp(-\beta V(x, y))$ corresponding to the effective potential V used for the mesoscopic description. Small values of the interaction parameter βV_s result in a diffuse ionic profile, similar to that of Na^+ (a), whereas larger values result in sharply peaked densities, mimicking the Cs^+ case (c). Inbetween, the resulting density is similar to the intermediate behaviour of K^+ (b). These profiles are to be compared to those obtained with the fully atomic description of figure 3.

FIG. 5: Mobility μ_{app} as a function of βV_s which characterizes the affinity of the ions for the surface. The value is rescaled by the "free" mobility $\mu_0 = 1/\gamma$ in absence of interactions with the surface. Results are given for the two components (x, y) of the mobility tensor, which reveal the isotropy of the honeycomb lattice. The mobility decreases with increasing interactions with the surfaces.

FIG. 6: Partitioning coefficient K_d as a function of the interaction parameter βV_s. The semi-logarithmic plot clearly reveals two regimes : For strong interactions with the walls or low temperature (right), the diffusion is activated (Arrhenius law); for weak interactions or high temperature (left), no such activated diffusion is seen. The solid line indicates the fit to an Arrhenius law with activation energy V_s.

Figure 1

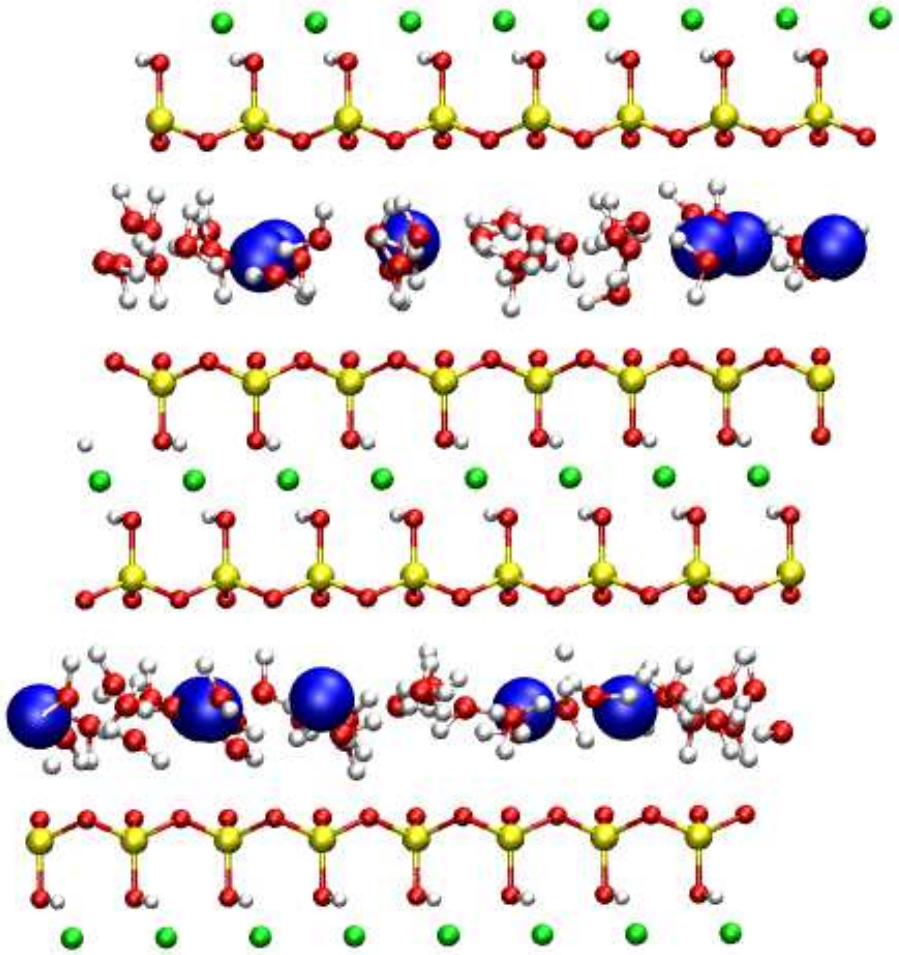

Figure 2

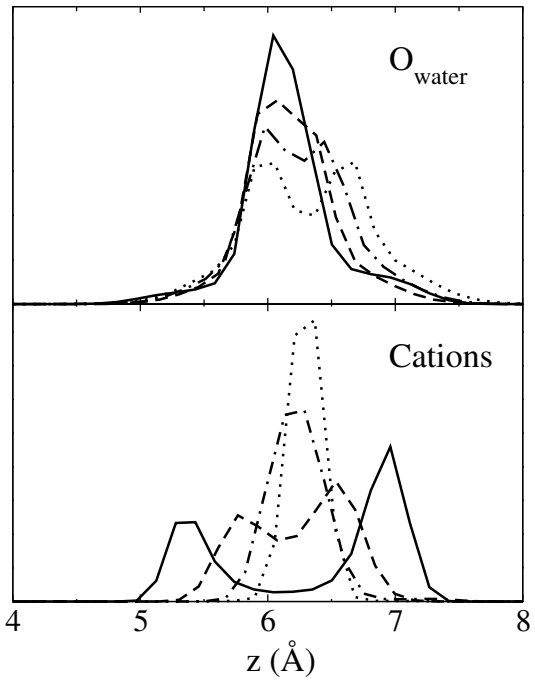

Figure 3

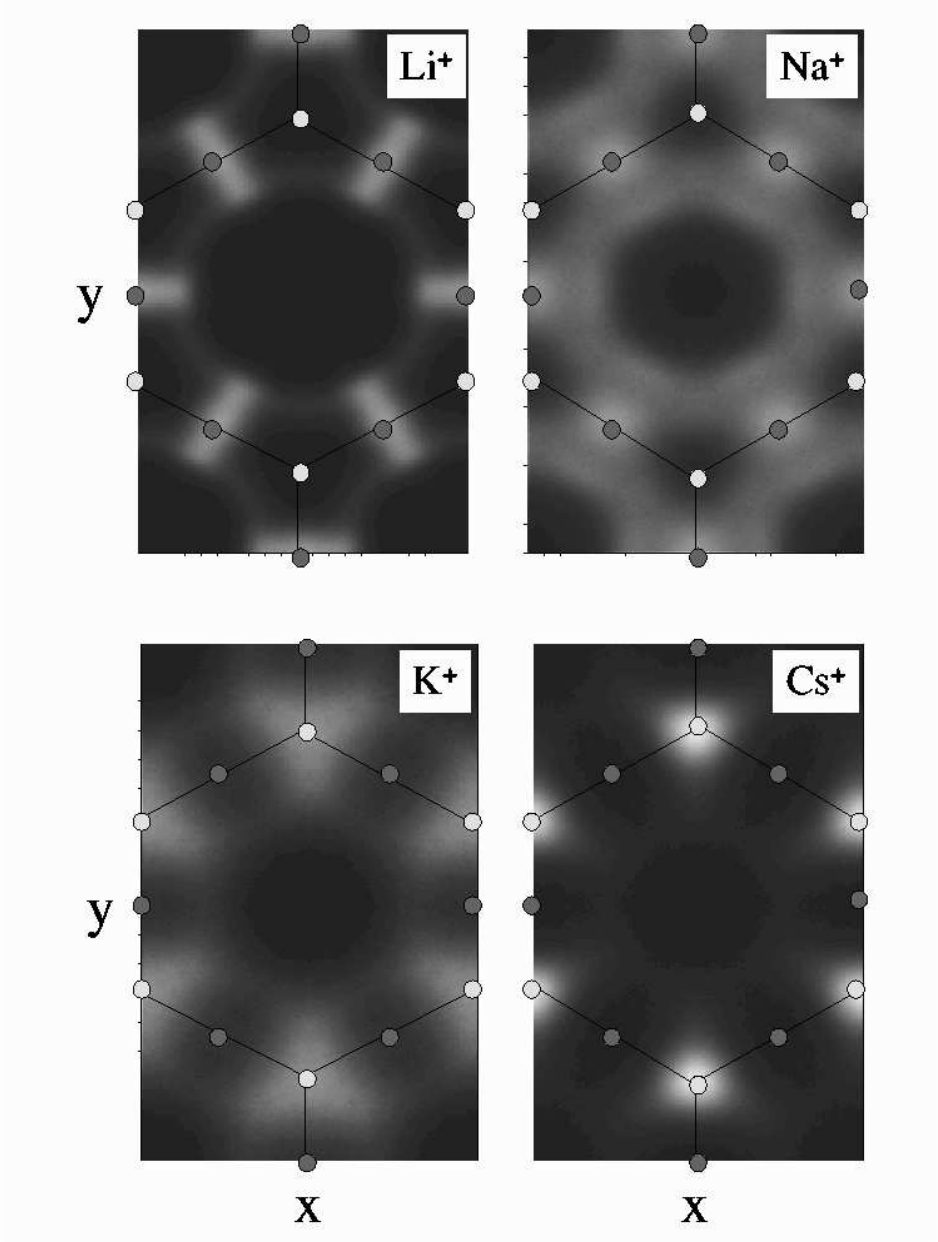

Figure 4

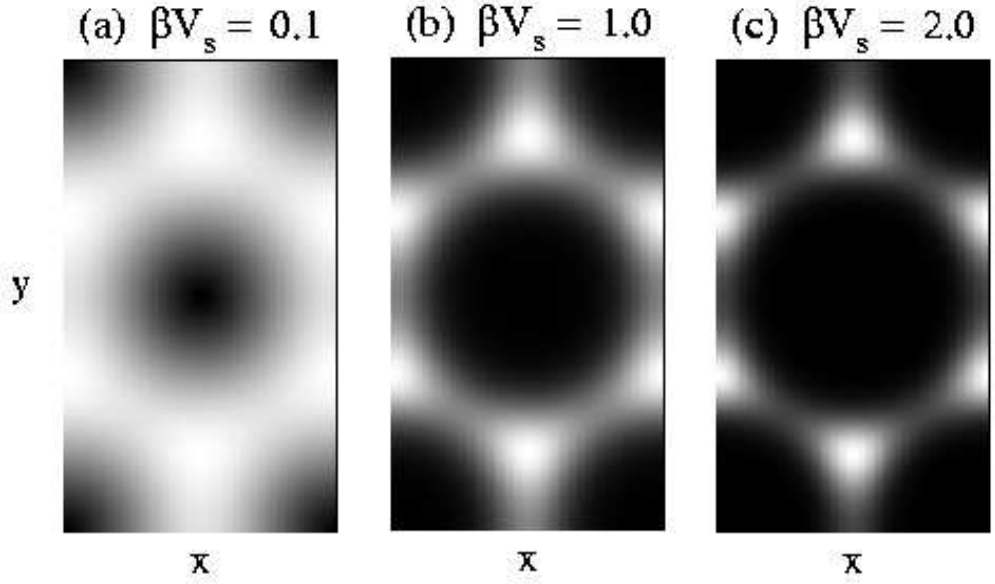

Figure 5

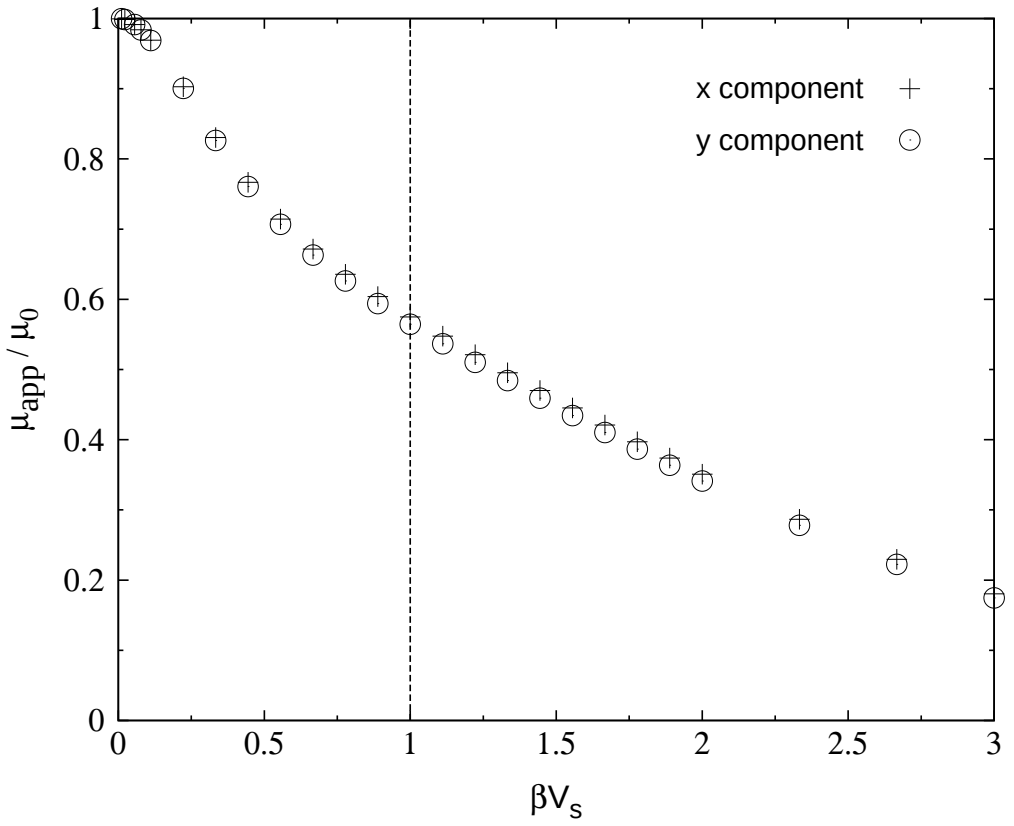
x component
y component
μ_{app} / μ_0
βV_s
0
0.2
0.4
0.6
0.8
1
0
0.5
1
1.5
2
2.5
3

Figure 6

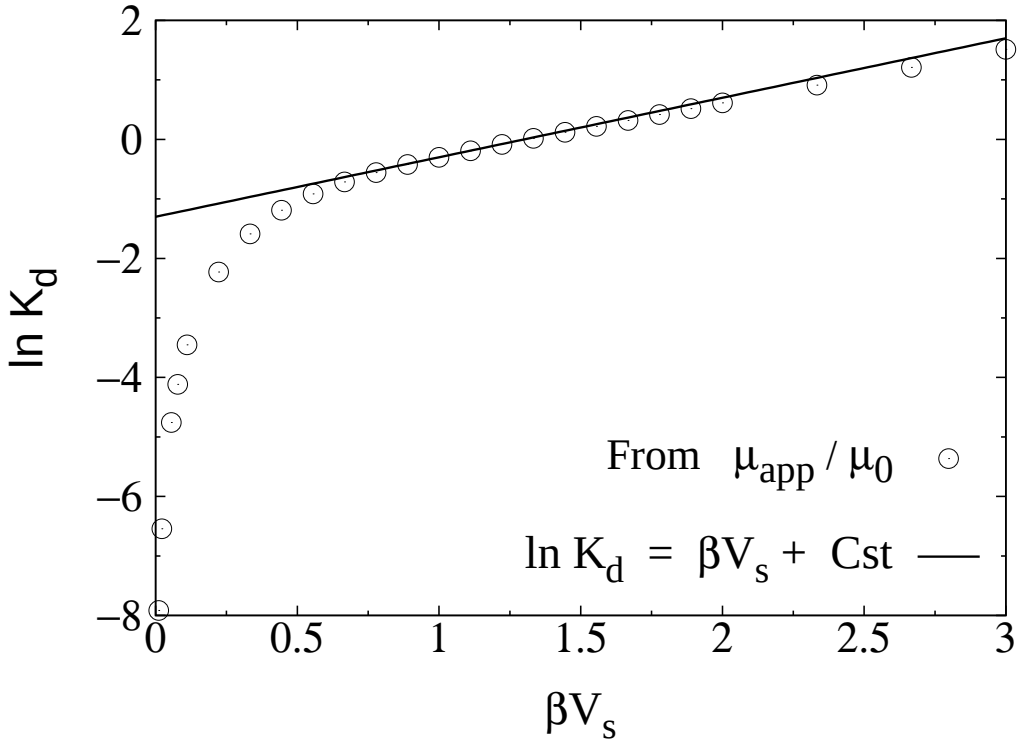
2
0
−2
−4
−6
−8
ln K_d
0
0.5
1
1.5
2
2.5
3
βV_s
From μ_{app} / μ_0
ln K_d = βV_s + Cst